Frontiers in Bioscience Landmark

Front. Biosci. (Landmark Ed) **2022**; 27(10): 290
https://doi.org/10.31083/j.fbl2710290

Original Research

A Combination of Native LC-MS Approaches for the Comprehensive Characterization of the Antibody-Drug Conjugate Trastuzumab Deruxtecan

Evolène Deslignière[1,2,3], Hélène Diemer[1,2,3], Stéphane Erb[1,2,3], Pierre Coliat[3,4], Xavier Pivot[3,4], Alexandre Detappe[3,4], Oscar Hernandez-Alba[1,2,3], Sarah Cianférani[1,2,3,*]

[1]Laboratoire de Spectrométrie de Masse BioOrganique, IPHC UMR 7178, Université de Strasbourg, CNRS, 67087 Strasbourg, France
[2]Infrastructure Nationale de Protéomique ProFI – FR2048, 67087 Strasbourg, France
[3]Strasbourg Drug Discovery and Development Institute (IMS), University of Strasbourg, 67000 Strasbourg, France
[4]Institut de Cancérologie Strasbourg Europe, 67000 Strasbourg, France
*Correspondence: sarah.cianferani@unistra.fr (Sarah Cianférani)
Academic Editor: Sukmook Lee
Submitted: 27 July 2022 Revised: 26 September 2022 Accepted: 29 September 2022 Published: 26 October 2022

Abstract

Background: Native mass spectrometry (nMS) approaches appear attractive to complement bottom-up strategies traditionally used in biopharmaceutical industries thanks to their quite straightforward and rapid workflows, especially through online hyphenation of non-denaturing liquid chromatography (LC) to nMS. The present work provides an overview of the state-of-the-art chromatographic tools available for the detailed characterization of monoclonal antibody (mAb) formats, exemplified on the antibody-drug conjugate (ADC) trastuzumab deruxtecan (T-DXd). **Methods**: T-DXd was first characterized by conventional reversed phase LC (rpLC) and peptide mapping. Couplings of size exclusion chromatography (SEC), cation exchange chromatography (CEX), and hydrophobic interaction chromatography (HIC) to nMS were used to gain further insights into size, hydrophobic, and charge variants of T-DXd and its parental mAb trastuzumab, at intact and middle-up levels. **Results**: SEC-nMS first offered a direct snapshot of the homogeneous conjugation of T-DXd, with an average drug-to-antibody ratio (DAR) of 8 in agreement with a conjugation on cysteines after reduction of all interchain disulfide bonds. Moreover, SEC-nMS afforded precise identification and quantification of aggregates and fragments. Middle-up level experiments performed after IdeS digestion confirmed that drug conjugation occurs in the Fab region of the mAb, as seen with rpLC. HIC separated two DAR8 species that could not be differentiated by nMS. Although middle-up HIC-nMS proved to be more informative for oxidized forms, the identification of minor variants was still difficult because of poor MS signal quality, showing how the coupling of HIC to nMS remains challenging. Lastly, middle-up CEX-nMS provided accurate determination and localization of post-translational modifications, with several acidic/basic variants within Fab and Fc regions of T-DXd that were also identified by peptide mapping. **Conclusions**: This study illustrates the strengths and drawbacks of each LC-nMS coupling. By combining SEC-, HIC-, and CEX-nMS, we were able to achieve a comprehensive characterization of T-DXd without extensive sample preparation prior to MS analysis.

Keywords: native mass spectrometry (MS); liquid chromatography (LC); size exclusion chromatography (SEC); cation exchange chromatography (CEX); hydrophobic interaction chromatography (HIC); higher order structures; biotherapeutics; antibody-drug conjugate (ADC)

1. Introduction

Over the last decade, antibody-drug conjugates (ADC) have evolved into promising and efficient therapeutic agents for targeted chemotherapy in cancers, with 11 and 9 ADCs currently approved by the Food and Drug Administration (FDA) and the European Medicines Agency (EMA), respectively, and more than 80 ADCs in clinical studies [1–3]. ADCs are generated through the conjugation of monoclonal antibodies (mAbs) targeting specifically the tumor-associated antigens (TAAs) of the tumor cell with highly potent cytotoxic drug payloads. Both elements are covalently bound *via* a cleavable or non-cleavable chemical linker [4]. While first-generation ADCs suffered from insufficient payload potency, high toxicity, and premature drug release [5], the second-generation ADCs (brentuximab vedotin BV, trastuzumab emtansine T-DM1) were designed with more potent payloads, improved linker stability, and lower levels of unconjugated mAbs [6]. Second-generation ADCs presented increased drug conjugation heterogeneity, with mixture of species ranging from 0 to 8 payload/mAb and average drug-to-antibody ratios (avDAR) of 3–4 through conjugation on primary amines of lysine side-chains (T-DM1) or cysteine thiol groups after reduction of the interchain disulfide bonds (BV) [7,8]. Hence, a third generation of ADCs that are more homogeneous in drug load polydispersity has been developed, yielding improved pharmacokinetics [1,2,9–12].

Among the recently approved ADCs, trastuzumab deruxtecan (T-DXd) consists of the humanized monoclonal anti-HER2 trastuzumab antibody, a cleavable, peptidyl-based linker stable in plasma (GGFG), and a potent topoisomerase I inhibitor payload (DXd, 1034 Da) [13,14]. T-DXd is used as monotherapy in third line treatment for patients with unresectable or metastatic HER2-positive breast cancer who have previously failed at least two lines of anti-HER2 therapy (trastuzumab/pertuzumab and T-DM1) [15]. T-DXd is produced using a conventional cysteine (Cys) conjugation strategy using a maleimide precursor drug targeting Cys residues of trastuzumab [13]. Briefly, disulfide bonds in the hinge region of trastuzumab are reduced using tris(2-carboxyethyl)phosphine hydrochloride (TCEP HCl), and the precursor drug linkers are added to the reduced mAb, leading to a DAR 8 with homogeneous conjugation, enabling efficient delivery of the payload to targeted cells [13,16].

The design of more potent and efficient ADC molecules has fostered analytical method development for their complete in-depth characterization. Generic chromatographic, electrophoretic and mass spectrometric methods employed either alone or in hyphenation are central in R&D process (from hit to lead optimization) [17–19]. Particular attention has been paid over the past 10 years to improve the speed and efficiency of analytical characterization throughout the development process. With recent implementation of native mass spectrometry (nMS) in R&D biopharmaceutical environments, an urgent need to have robust, reproducible, and automated liquid chromatography coupled to nMS (LC-nMS) methods has emerged [19,20]. Among those, size exclusion chromatography coupled to nMS (SEC-nMS) has emerged first as an analytical methodology that is appropriate for accurately quantifying the drug-to-antibody ratio (DAR) on a wide variety of interchain Cys-linked ADCs, irrespective of the chemotype [21–24]. Hydrophobic interaction chromatography (HIC) is also frequently employed for the characterization of biopharmaceutical products presenting varying degrees of hydrophobicity. HIC has become the gold standard technique to determine the avDAR and drug load distribution (DLD) of Cys-ADCs conjugated to hydrophobic payloads. Optical detection methods are most commonly used in combination with HIC because coupling to MS is highly challenging due to high ionic strength (>2 M). Recent developments have thus aimed at interfacing HIC to nMS through unidimensional [25–27] or bidimensional [28] setups, which afforded HIC separation and MS identification of DAR species from Cys-ADCs, even allowing to differentiate positional isomers [27,28]. The biopharma analytical toolbox also comprises cation exchange chromatography (CEX), which is a powerful method to separate species with different surface charges, including deamidated forms. The charge of the mAb is modified if the drug or linker possess charge or if they neutralize/hide existing charge of the mAb upon binding, which makes CEX-nMS an appealing technique for the characterization of ADCs [29,30].

Here we used T-DXd, a last-generation homogenous Cys-ADC with a high DAR, as a model compound to illustrate the potentials of state-of-the-art LC methods coupled to nMS, with a focus on discussions about the benefits and pitfalls of each analytical workflow.

2. Materials and Methods

2.1 Samples and Enzymes

Trastuzumab and T-DXd samples were provided by the Institut de Cancérologie Strasbourg Europe (Strasbourg, France).

2.2 Sample Preparation

For middle-up level experiments, IdeS digestion was performed by incubating one unit of FabRICATOR enzyme (Genovis, Lund, Sweden) per microgram of mAb or ADC for 60 min at 37 °C.

2.3 Denaturing Approaches

Detailed protocols for peptide mapping and rpLC-MS are available in SI (**Supplementary Text 1** and **Supplementary Text 2**, respectively).

2.4 SEC-nMS Experiments

An Acquity UPLC H-class system (Waters, Wilmslow, UK) composed of a quaternary solvent manager, a sample manager set at 10 °C, a column oven and a TUV detector operating at 280 nm and 214 nm was coupled to an Orbitrap Exactive Plus EMR mass spectrometer (Thermo Fisher Scientific, Bremen, Germany) equipped with an Ion Max source with a heated electrospray ionization HESI probe. 20 and 10 μg were injected for intact and middle-up level analyses, respectively. The SEC column used was an ACQUITY Premier Protein SEC 250 Å, 1.7 μm, 4.6 $\times$ 150 mm (Waters). The separation was carried out in isocratic mode with a 50 mM $AcONH_4$ mobile phase at pH 6.9. The flowrate was set to 250 μL/min and 150 μL/min for intact and middle-up analyses, respectively. The ESI parameters were set as follows: sheath gas flowrate to 30 a.u., auxiliary gas flowrate to 10 a.u., ion transfer capillary temperature to 250 °C, vaporizer temperature to 150 °C, and capillary voltage 4.0 kV. The S-lens RF level was set to 200%. In-source collision induced dissociation (CID) and higher-energy collisional dissociation (HCD) energies were set to different values along the elution for intact-level experiments, in order to achieve an optimal desolvation for each species: 90/100 eV (CID/HCD) for dimers, 100/10 for monomers, and 80/10 for fragments <100 kDa. For middle-up level analyses, CID/HCD energies were lowered to 50/10 eV. The trapping gas pressure was 7 a.u. (corresponding to an ultra-high vacuum of 1e-9 mbar). The voltages on the injection, inter, and bent flatapoles were tuned to 8, 7, and 6 V, respectively. Acquisitions were performed

in the *m/z* range 1000–12,000 with a 3 s scan time and a resolution of 35,000 (17,500 for dimers) at 200 *m/z*. The automatic gain control (AGC) target was set to 1e6, and the maximum injection time was 300 ms. Data were interpreted using MassLynx v4.1 (Waters, Milford, MA, USA) and BioPharma Finder v3.2 (Thermo Fisher Scientific, San Jose, CA, USA). The deconvolution mass tolerance was set to 10 ppm.

2.5 HICxSEC-nMS Experiments

The online 2D HICxSEC-nMS setup has been extensively described elsewhere [28]. The HIC column was a MAbPac HIC-10, 1000 Å, 5 μm, 4.6 $\times$ 100 mm (Thermo Fisher Scientific). The SEC column used in the second dimension was an AdvanceBio SEC 300 Å, 2.7 μm, 4.6 $\times$ 50 mm (Agilent Technologies, Santa Clara, CA, USA). 200 and 150 μg were injected for intact and middle-up level analyses, respectively. For the first dimension (HIC), the mobile phase A was composed of 2.5 M of $AcONH_4$ and 0.1 M phosphate buffer (Na_2HPO_4) at pH 7.0 (adjusted with phosphoric acid), whereas the mobile phase B was composed of 0.1 M phosphate buffer (Na_2HPO_4 and NaH_2PO_4) with pH 7.0 (adjusted with a NaOH solution). The following gradient was employed in HIC: 0 to 90% B in 36 min, 90 to 100% B in 21 min, then maintained at 100% B for 8 min before re-equilibration for 25 min, leading to a total analysis time of 90 min. The HIC experiment was conducted at a flowrate of 100 μL/min. Column temperature, wavelength, and data acquisition rate were set to 30 °C, 280 nm, and 10 Hz, respectively. For the second dimension (SEC), the separation was carried out in isocratic mode with 100 mM $AcONH_4$at pH 6.9, usinga flowrate of 700 μL/min. Column temperature, wavelength, and data acquisition rate were set at 25 °C, 210/280 nm, and 40 Hz, respectively. The analysis time of the second-dimension run corresponds to the sampling time of the first-dimension separation (1.5 min). In order to limit salt contamination of the ESI source, a fraction of 0.45 min is sent to MS thanks to a switching valve. A flow splitter was employed to reduce the flowrate to 100 μL/min prior to MS analysis.

The Synapt G2 HDMS mass spectrometer (Waters, Manchester, UK) was operated in sensitive mode and positive polarity with a capillary voltage of 3.0 kV. The cone voltage and backing pressure were set to 120 V and 6 mbar, respectively, to preserve noncovalent interactions. Source and desolvation temperature were held to 100 and 450 °C, respectively. Desolvation and cone gas flows were 750 and 60 L/h, respectively. Acquisitions were performed in the *m/z* range of 1000–10,000 with a 1.5 s scan time. Data were analyzed with MassLynx v4.1.

2.6 CEX-nMS Experiments

CEX-nMS analyses use the same LC-MS system as SEC-nMS experiments (Acquity H-Class coupled to the Orbitrap Exactive Plus EMR). The CEX column was a YMC-BioPro 5 μm, 4.6 $\times$ 100 mm (YMC, Dinslaken, Germany). 63 and 31 μg were injected for intact and digested samples, respectively. The mobile phase A was composed of 20 mM $AcONH_4$ at pH 5.6, while the mobile phase B contained 140 mM $AcONH_4$ and 10 mM NH_4HCO_3 at pH 7.4. For intact samples, the following gradient at a flowrate of 250 μL/min was used: 40 to 50% B in 2 min, 50 to 70% B in 11.5 min, increase to 100% B in 0.1 min and maintained for 5.4 min, followed by a re-equilibration step of 3 min. For middle-up level analyses, the %B was increased from 10 to 100% in 16 min, and kept at 100% for 4 min, at a flowrate 0.25 μL/min. MS parameters were identical to SEC-nMS experiments, except for CID/HCD values which were set to 120/10 eV for intact-level analyses. Data were interpreted using BioPharmaFinder v3.2. The deconvolution mass tolerance was set to 10 ppm.

3. Results and Discussion

3.1 Classical MS-Based Characterization of T-DXd Drug Substance

Intact mass analysis in denaturing conditions— Intact-level analysis consists of measuring the mass of the full mAb/ADC, generally by classical denaturing reversed phase LC (rpLC) using C8 or C4 columns, coupled to denaturing MS. As rpLC-MS is implemented in most labs, it can be routinely performed to provide accurate intact mass measurements. rpLC-MS is particularly well adapted for mAbs and highly homogeneous ADC formats, but it might be trickier for heterogeneous ADC [31], or even ADCs partially or completely constituted of noncovalent assemblies, such as BV [32] or T-DXd. In absence of interchain disulfide bonds, the light chain bearing one drug (24,472.8 $\pm$ 0.1 Da) and the heavy chain containing three drugs (53,696.4 $\pm$ 0.2 Da) are observed (Fig. 1A). For each subunit, a minor peak associated to a fragmentation within the payload (–475 Da) was also detected. In addition, a minor species with a mass of 24,473.6 $\pm$ 0.4 Da was observed for the light chain, which may correspond to a deamidation (Fig. 1A). For the heavy chain, an oxidized form was also detected (53,714.4 $\pm$ 0.5 Da) as a shoulder. However, no species corresponding to free light or heavy chains was detected with rpLC-MS, suggesting an avDAR of 8.0. In addition, rpLC-MS can also give a direct snapshot of the glycosylation profile, and revealed four glycoforms for T-DXd, namely G0F-N/G0F, G0F/G0F (major one), G0F/G1F, and G1F/G1F.

Middle-up level subunit analysis in denaturing conditions—To precise the localization of drug conjugation and because mass measurements performed by rpLC-MS are more accurate for lower masses, downsizing of $>$150 kDa intact ADC can be achieved using a variety of enzymes [33–36] that specifically cleave the mAb format into smaller subunits. After IdeS enzymatic digestion, which cleaves mAbs below the hinge region, three major species corresponding to the light chain with one drug (24,472.9 $\pm$ 0.1 Da), Fd subunit linked to three drugs (28,481.2 $\pm$ 0.2

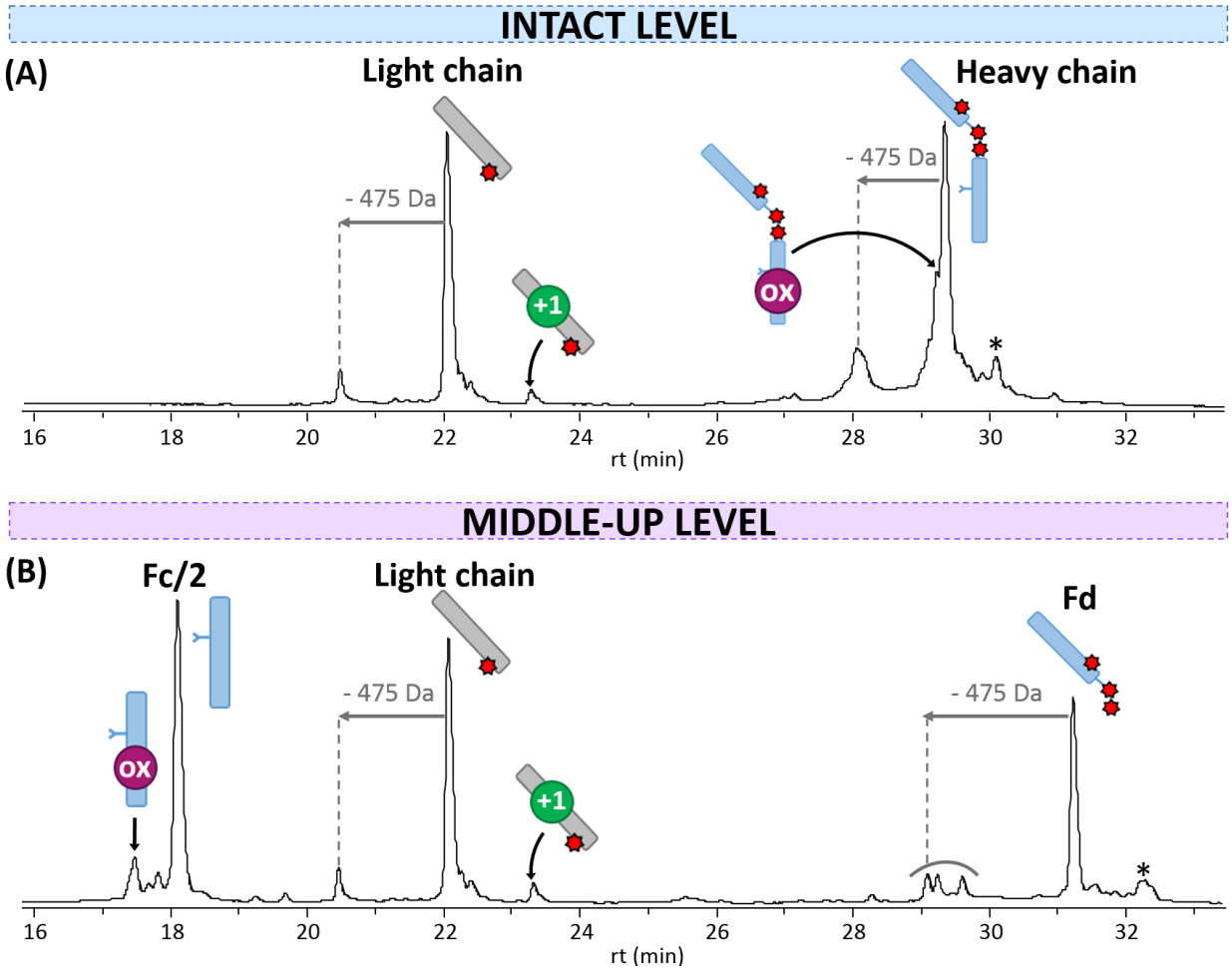

Fig. 1. rpLC-MS analysis of T-DXd. Chromatograms obtained (A) at the intact level, and (B) at the middle-up level after IdeS digestion. mAb cartoons with colored dots were used to represent the modifications corresponding to each PTM: oxidation (ox, pink) and deamidation (+1 Da species, green). Drugs are represented with red stars. * = loss of 44 Da.

Da), and unconjugated Fc/2 region (25,232.7 ± 0.1 Da for the G0F/G0F glycoform) were observed (Fig. 1B). No signals associated to the light chain or Fd without any bound DXd could be detected from extracted ion chromatograms (avDAR = 8.0), in agreement with intact rpLC-MS results. Middle-up analysis thus allowed confirming the localization of all drugs on the upper region of the mAb, being consistent with the position of the interchain disulfide bridges of the naked mAb. One minor species identified as the Fc/2 subunit bearing 1 oxidation was also observed.

Bottom-up level peptide mapping analysis—Finally, bottom-up strategies are conventionally used in biopharmaceutical environment to obtain sequence information and localize modification sites [37]. Peptide mapping performed on T-DXd after digestion with two different enzymes (trypsin and pepsin) resulted first in a sequence coverage of 96% for the heavy chain and 100% for the light chain, confirming the primary amino acid sequence. Several post-translational modifications (PTMs) were also detected in both chains (Fig. 2, Table 1). More precisely, the light chain contains two modifications: one methionine oxidation (M4, noted ox), and one deamidation (on residues Q27, N30, Q37, and/or Q38—in particular, N30 is known to be responsible for charge heterogeneity in the parent mAb trastuzumab [38,39]). The heavy chain comprises five modifications: the formation of pyroglutamate from the N-terminal Glu (E1, called pyroGlu), two methionine oxidations (M83 and M255), an aspartate isomerization (D283, referred to as isoAsp), and the presence of a C-terminal lysine (K450). Of note, no peptide corresponding to the succinimide ring opening (+18 Da on the payload) [40] was detected on the reference compound. Finally, conjugation was confirmed at positions C223, C229, and C232 on the heavy chain, and C214 on the light chain, in agreement with a Cys-conjugation strategy following reduction of interchain disulfide bonds (Fig. 2). Peptides comprising the conjugated Cys residues could be identified with both the intact (1034 Da) and fragmented (–475 Da) payloads, in line with rpLC-MS data.

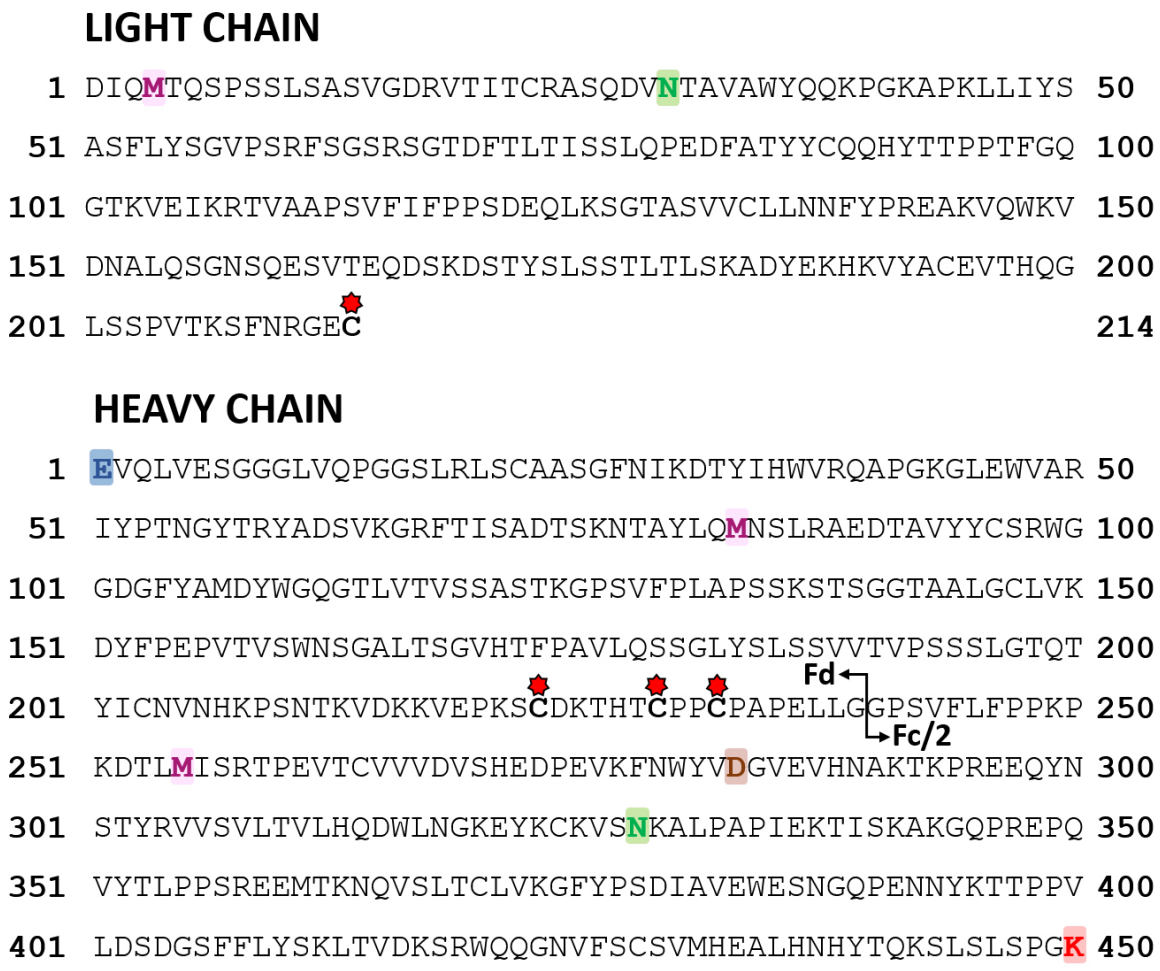

Fig. 2. Sequence of T-DXd. Modifications identified in peptide mapping are in bold (blue = pyroGlu; pink = oxidation; brown = isoAsp; green = deamidation; red = C-terminal Lys). Drug conjugation sites at cysteine residues are indicated with red stars. The IdeS cleavage is represented by a black arrow.

Table 1. Summary of PTMs identified with peptide mapping.

Region	Residue	Modification	Peptide	Reference	Stressed
Light chain	M4	Oxidation	DIQ**M**TQSPSSLSASVGDR	18 ± 4%	18 ± 1%
	Q27-N30-Q37-Q38	Deamidation	AS**Q**DV**N**TAVAWY**QQ**KPGKAPK	12 ± 1%	18 ± 1%
Fd	E1	PyroGlu	**E**VQLVESGGGLVQPGGSLR	1 ± 1%	4 ± 1%
	M83	Oxidation	NTAYLQ**M**NSLR	9 ± 1%	9 ± 1%
Fc/2	M255	Oxidation	DTL**M**ISR	47 ± 1%	49 ± 5%
	D283	isoAsp	FNWYV**D**GVEVHNAK	1 ± 1%	18 ± 1%
	N328	Deamidation	VS**N**KALPAPIEK; VS**N**KALPAPIEKTISK	<1%	10 ± 1%
	K450	C-terminal Lys	SLSLSPG**K**	23 ± 1%	19 ± 1%

Proportions reported in the two last columns represent the percentage of modified form for each peptide. The color code associated to each PTM is the same for all figures: oxidation = pink; deamidation = green; pyroGlu = blue; isoAsp = brown; C-terminal Lys = red.

3.2 Native MS-Based Characterization of T-DXd Drug Substance

SEC-nMS for size variants analysis—Aggregates (high molecular weight species, HMWS) and fragments (low molecular weight species, LMWS) are critical quality attributes that have to be characterized for ADCs, conventionally by SEC-UV [41]. Data interpretation is thus only based on peak retention times. Recent development of SEC-nMS has paved the way for more accurate, less time-consuming all-in-one HMWS/LMWS assignment along with drug substance characterization [22,42].

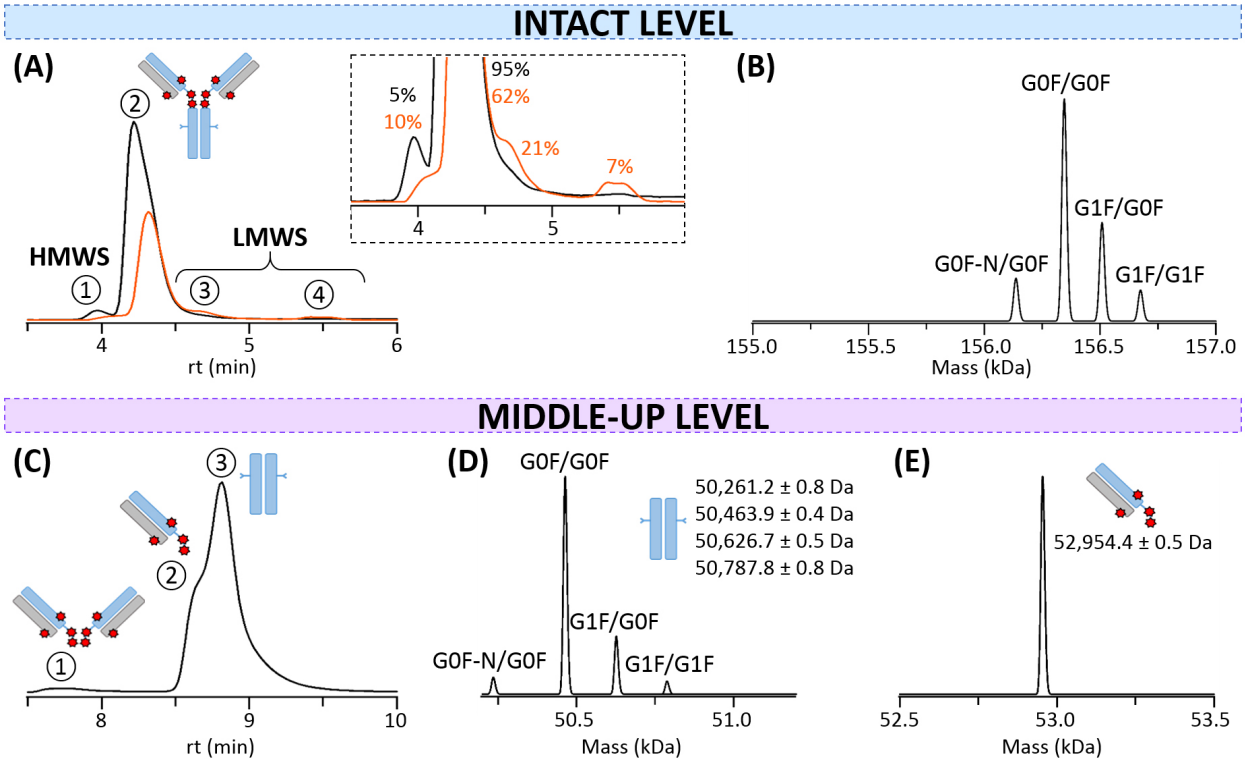

Fig. 3. SEC-nMS analysis of T-DXd. (A) SEC-UV chromatograms of intact (black) and thermally-stressed (orange) T-DXd. Inset: Focus on minor species and their corresponding relative amounts. (B) Mass deconvolution of the intact monomer (peak 2) for the non-stressed sample. (C) SEC-UV chromatogram of IdeS-digested non-stressed T-DXd. (D) Mass deconvolution of the Fc subunit. (E) Mass deconvolution of the Fab region.

Table 2. SEC-nMS mass measurements of intact T-DXd.

HMWS	Main product				LMWS	
①Dimer	② Monomer		③Fc-Fab		④ Fragments	
312,797 ± 8 Da	G0F-N/G0F	156,134 ± 4 Da	C223DKT/**HTC229**	106,810 ± 3 Da		
	G0F/G0F	156,339 ± 1 Da	CDK/**THTC**	106,924 ± 4 Da	Free light chain	24,473.2 ± 0.2 Da
		156,376 ± 1 Da	CD/**KTHTC**	107,023 ± 1 Da		
	G1F/G0F	156,501 ± 3 Da	C/**DKTHTC**	107,135 ± 2 Da		
		156,531 ± 5 Da			Dimeric light chain	48,946.0 ± 0.5 Da
	G1F/G1F	156,664 ± 4 Da				

Additional species generated upon thermal stress are reported in orange.

Intact glycosylated T-DXd was thus first analyzed using SEC-nMS. The main peak corresponds to monomeric T-DXd (peak 2, >95% based on the SEC-UV chromatogram) with its glycoforms (Fig. 3A). A mass of 156,339 ± 1 Da was measured for the main glycoform G0F/G0F of the monomer (Fig. 3B, Table 2), in good agreement with the mAb bearing 8 conjugated drugs (expected mass of 156,339 Da for G0F/G0F). Overall, the straightforward spectrum of T-DXd resulting from homogeneous Cys-conjugation affords easy DAR determination, as opposed to heterogeneous second-generation ADCs such as T-DM1 or BV which present highly complex spectra (**Supplementary Fig. 1**). In addition, the use of a novel bioinert SEC column (see Materials and Methods) that minimizes secondary interactions between the analyte and the stationary phase proved to be particularly interesting here, as it has been shown to yield more reliable HMWS/LMWS quantification [43]. Low amounts of HMWS were detected at lower retention times (~4 min) and attributed to dimers bearing a total of 16 drugs from the mass measurement (peak 1) (Fig. 3A, Table 2), while no significant amounts of LMWS (<1%) were detected at greater elution volumes.

As mass accuracies are superior for lower size analytes, SEC-nMS experiments were also performed after enzymatic IdeS digestion. Additionally, this approach enables a more precise overview of the localization of the drugs on the different parts of the mAb (Fab and Fc). Hence, two major species attributed to Fab and Fc subunits are par-

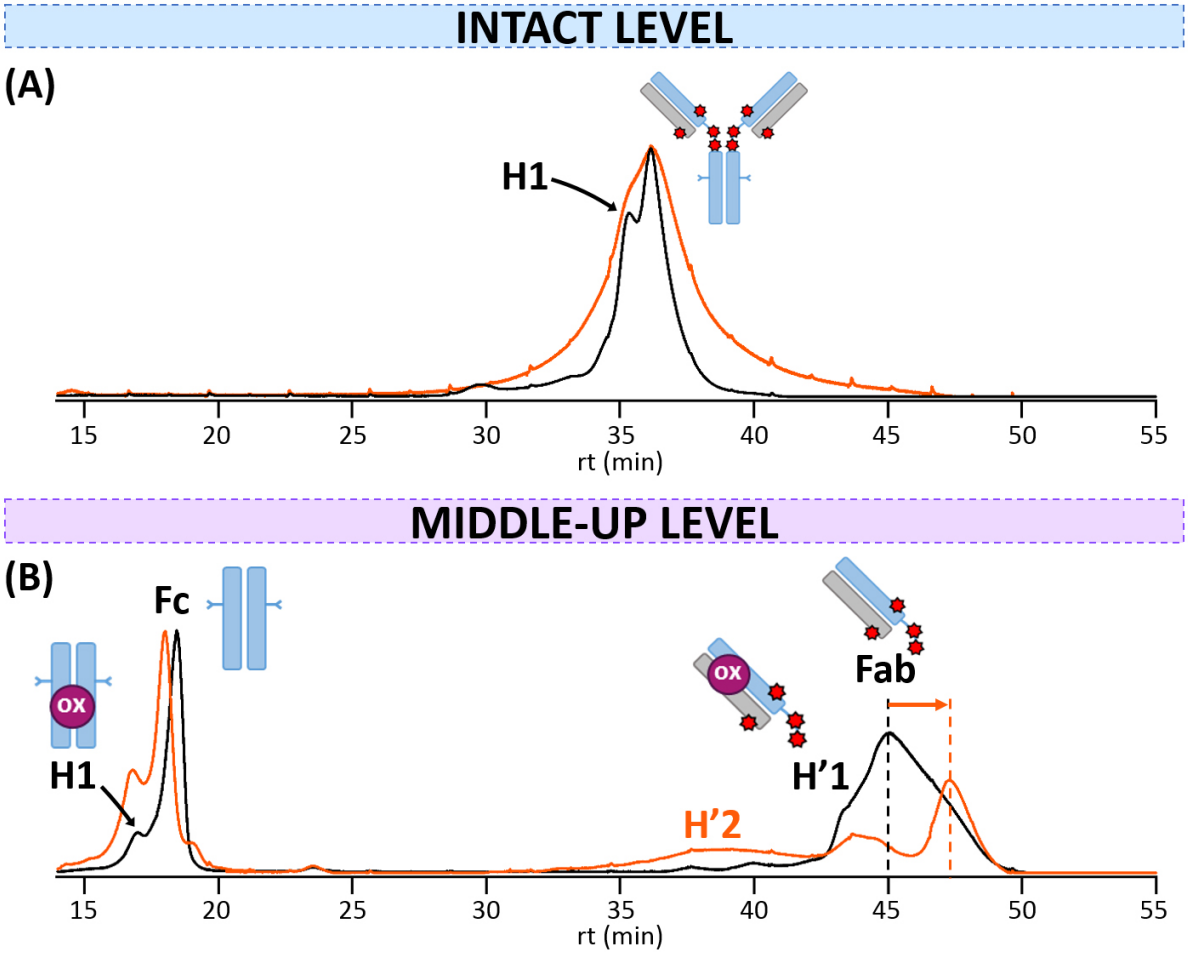

Fig. 4. HICxSEC-nMS analysis of T-DXd. HIC-UV chromatograms of reference (black) and thermally-stressed (orange) T-DXd obtained (A) at the intact level, or (B) at the middle-up level. mAb cartoons with colored dots were used to represent the modifications corresponding to each charge variant: oxidation (ox, pink).

tially separated on the SEC column (Fig. 3C). The Fc subdomain (peak 3) presents a baseline-resolved glycoforms profile without any drug attached (50,463.9 ± 0.4 Da for the major glycoform G0F/G0F, Fig. 3D), in agreement with all previous LC-MS data. As expected, each Fab fragment contains 4 payloads (peak 2, 52,954.4 ± 0.5 Da, Fig. 3E). Note that the $F(ab')_2$ subdomain, eluted in peak 1, only accounts for 4% of the UV signal. As all interchain disulfide bonds have been reduced during the conjugation process, the $F(ab')_2$ subdomain is supposed to be held only by non-covalent interactions and appears to partially dissociate at the hinge region, leading to the release of the Fab part.

HICxSEC-nMS for drug conjugation assessment—As HIC is the gold standard for Cys-ADC analysis to assess DLD, we next moved to HIC-nMS analysis of T-DXd using our previously developed bidimensional HICxSEC-nMS methodology [28].

For the naked parent trastuzumab, a unique population corresponding to the unmodified monomer (148,385 ± 5 Da) is eluted at ~22.4 min (**Supplementary Fig. 2A**). T-DXd possesses 8 drugs and is eluted significantly later, at approximately 36 min. Two main populations are partially separated at the intact level for T-DXd (Fig. 4A). The peak at ~36.2 min corresponds to the monomer bearing 8 drugs (156,500 ± 1 Da), in agreement with the major DAR8 species detected using SEC-nMS. The more hydrophilic variant H1 at ~35.4 min could not be clearly mass-identified due to coelution with the main form. It is likely that other variants are comprised within the main broad peak (FWHM = 2 min *versus* 0.91 min for T-DXd and trastuzumab, respectively), and so performing HIC at the middle-up level may help to decipher the HIC profile of intact T-DXd.

After IdeS digestion, the HIC profile of T-DXd is more populated compared to the intact level, as several variants are uncovered for both subunits. The Fc region elutes first at ~17.9 min (same time as the naked mAb, **Supplementary Fig. 2B**), as all hydrophobic drugs retained by the HIC stationary phase are localized on Fab subunits of T-DXd. Two species are separated within the Fc region: the major unmodified species (50,466 ± 2 Da), and a hydrophilic variant (H1) with one oxidation (50,481 ± 3 Da, Fig. 4B), consistent with rpLC-MS results already reported. The Fab sub-

unit profile consists of a main unmodified species bearing 4 intact drugs (52,955 ± 1 Da), and one hydrophilic variant H'1 containing an oxidation (52,974 ± 2 Da). Neither species bearing lower numbers of drugs nor free unconjugated Fab forms were detected.

These results clearly show that the online coupling of HIC separation to nMS remains challenging. For Cys-ADC, it is highly desirable that the separation profile achieved from a HIC-nMS method is comparable to that from more conventional HIC-UV methods, so that valuable information from MS analysis could be directly applied to assist peak assignment and identity elucidation. While our 2D HICxSEC-nMS strategy successfully enabled online coupling of HIC to nMS in an indirect manner but with optimal chromatographic performances, the MS sampling resolution from the HIC separation remains limited by the run time of the second dimension (1.5 min), which happens to be problematic to differentiate species with very close retention times. Additionally, because samples are diluted along elution in the HIC and SEC columns, the intensity of the MS signal may be too low for an accurate determination of variants. Nonetheless, we were able to clearly assign intense hydrophilic oxidized forms, which are particularly amenable to HIC separation as seen with unidimensional HIC-nMS [26].

CEX-nMS for charge variants—We next aimed at analyzing charge variants of T-DXd to provide a more comprehensive analysis of the ADC, with an accurate identification of PTMs. The mAbs generally exhibit a high level of heterogeneity, due to their PTMs and their susceptibility to chemical and physical degradations. Among the chemical degradations, oxidation, deamidation, isomerization, glycation, succinimide ring opening etc., have to be monitored and quantified in the drug substance since those modifications are often related to immunogenic effects, thus impairing patient safety [44].

The first experiments performed on the parental mAb trastuzumab demonstrate the presence of three distinct species (**Supplementary Fig. 3A**): (i) a major unmodified species, (ii) one acidic variant corresponding to a deamidation, and (iii) a basic variant identified as an isoAsp, in agreement with several already published studies [39,45–47]. As T-DXd is derived from a neutral hydrophobic drug (DXd), CEX charge profiles of trastuzumab and T-DXd should be similar under identical experimental conditions. Interestingly, T-DXd presents a different profile characterized by a broad major peak at ~17.9 min (FWHM = 0.45 *versus* 0.16 min for T-DXd and trastuzumab, respectively) and a poor resolution of separation with substantial fronting (Fig. 5A). This result stems from secondary interactions between the ADC and the stationary phase mainly driven by the hydrophobic interactions with the hydrophobic drugs of T-DXd, thus being detrimental to the quality of the CEX separation [29,30,48]. Despite this lack of chromatographic resolution, nMS sensitivity and accuracy enabled the assignment of different species: a major form (M) whose glycoform and drug load profiles are consistent with the one observed in SEC-nMS for T-DXd (see inset in Fig. 5A), two acidic variants comprising one (A1) or two (A2) oxidations, and a basic variant (B1) which may be linked to an isoAsp (Table 3A), all bearing 8 drugs. It is likely that other PTMs are present, but could not be identified due to poorly resolved chromatographic separation. Again, no species with lower DAR values were detected in intact CEX-nMS analysis.

Overall, both the inherent charge heterogeneity and drug hydrophobicity of the ADC make it challenging to interpret the CEX profile of intact T-DXd, highlighting some limitations of CEX analysis for hydrophobic ADCs. In addition, unambiguous isoAsp (+0 Da) or deamidation (+1 Da) identification is often not achieved at the intact level as mass shifts fall within the margin of measurement error. As a result, PTM assignment strongly relies on associated retention shift (isoAsp = basic variant, deamidation = acidic variant). Thus, middle-up level analyses are generally more adapted for a more precise characterization of charge variants [49,50].

Analyzing IdeS-digested subunits with CEX-nMS affords clear benefits over intact-level experiments, providing localization of charge size variants along with more accurate mass measurements to ease PTM assignment. For trastuzumab, the middle-up level CEX profile accurately mirrors PTMs observed at the intact level with a chromatographic resolution comparable to that of intact trastuzumab (**Supplementary Fig. 3B**). The deamidations and isoAsp previously identified at the intact level occur on the $F(ab')_2$ region, as reported in another study [51]. Advantages of performing CEX-nMS at middle-up level are obvious for T-DXd as distinct chromatographic peaks are now observed. The peak width of the Fc subunit peak becomes thinner (FWHM = 0.12 min, equal to trastuzumab) compared to the intact profile, as the contribution of drug hydrophobicity is now avoided (no drug on the Fc subunit). On the other hand, the Fab region still displays a broad peak with significant fronting (Fig. 5B), in part explained by the increasing ionic strength over elution time. Indeed, low ionic strength mobile phases focus chromatographic peaks, whereas higher ionic strength leads to broader peaks [52]. Five different basic variants are observed for the Fc subunit: B1 may be related to an isoAsp, B2 and B5 contain one and two oxidations, respectively, while B3 and B4 correspond to the presence of one or two C-terminal Lys (+128 Da) (Fig. 5B, Table 3B). The Fab subunit has two acidic variants, associated to an oxidation (A'1) and two deamidations (A'2). One minor basic species resulting from a N-terminal pyroglutamate (B'1) is also observed. All Fab variants bear 4 drugs in addition to the PTMs. These experiments particularly highlight that the ADC (here T-DXd) is more prone to oxidation than its naked counterpart (here trastuzumab). More importantly, all PTMs identified with peptide map-

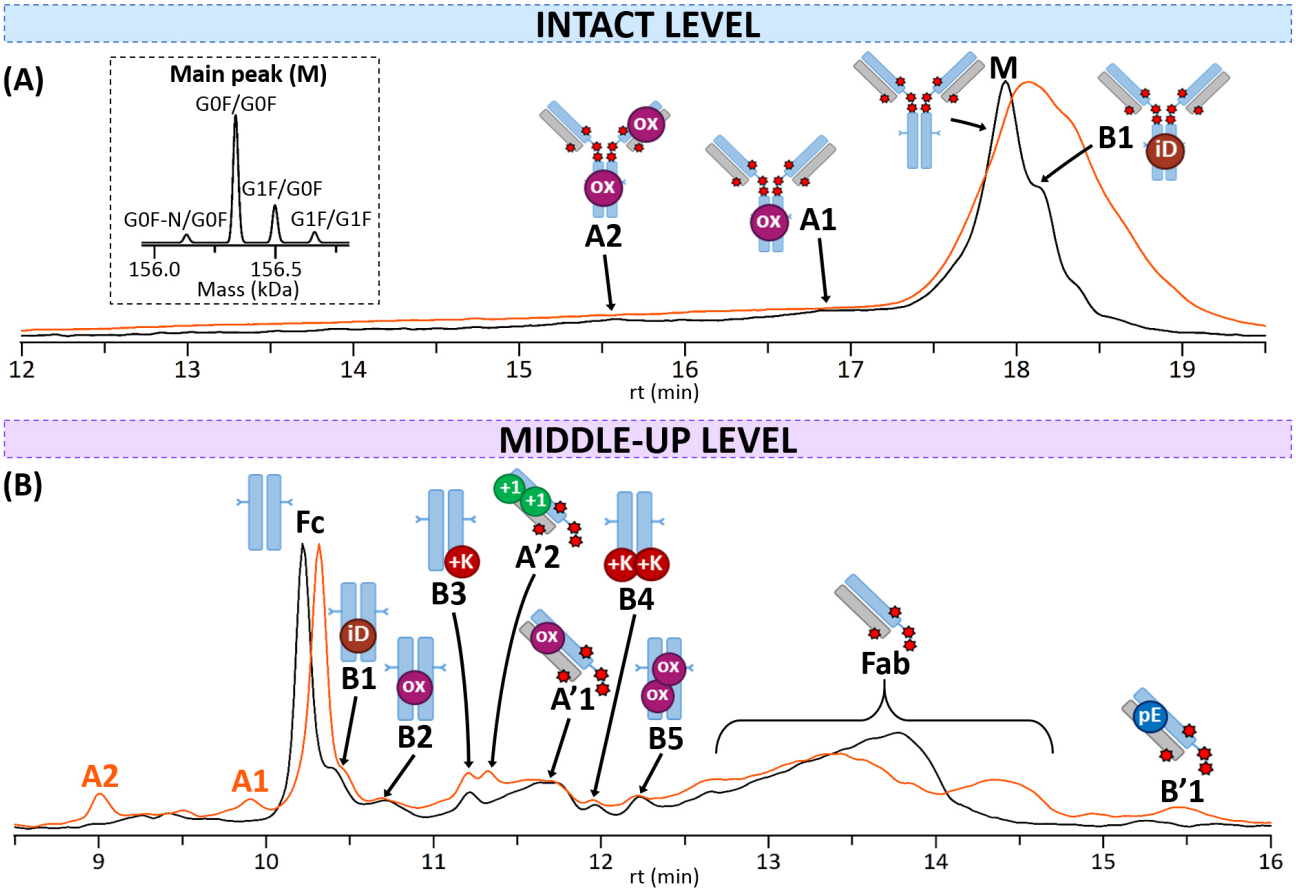

Fig. 5. CEX-nMS analysis of T-DXd. CEX-UV chromatograms of reference (black) and thermally-stressed (orange) T-DXd obtained (A) at the intact level (inset: focus on MS deconvolution of the main peak M), or (B) at the middle-up level. Acidic variants are indicated with the letter A and basic variants with the letter B. mAb cartoons with colored dots were used to represent the different modifications corresponding to each charge variant: oxidation (ox, pink), isoAsp (iD, brown), C-terminal Lys (+K, red), pyroGlu (pE, blue), deamidation (+1, green).

ping were also detected with middle-up CEX-nMS analysis, confirming the suitability of CEX to identify PTMs in a rapid manner without extensive prior sample preparation. Hence, the CEX-nMS method represents a significant advantage over bottom-up strategies which require considerable sample treatment that may generate artifactual PTMs.

3.3 Forced Degradation Studies

Forced degradation studies are essential for the development of therapeutic proteins to evaluate their stability in different conditions (storage, time, temperature, etc.) [53]. They can also be of interest in analytical method development and validation. In forced degradation conditions, minor species can be either artificially generated or enriched, constituting an interestingly more complex analytical matrix. For therapeutic mAbs, forced degradation studies highlight hot spots or points of fragility of proteins (deamidations, oxidations, aggregation, fragments, etc.) while simultaneously ensuring that the developed analytical methods are able to detect them. We thus thermally stressed T-DXd (15 days at 50 °C) and evaluated our different LC-nMS workflows for the detection of new low amount proteoforms.

Peptide mapping—We first performed classical bottom-up peptide mapping analysis as reference method to precisely identify and quantify PTMs generated in forced degradation conditions. Upon thermal stress, an additional deamidation site is observed within T-DXd, at position N328 on the heavy chain (Fig. 2, Table 1), along with a peptide from the hinge region with succinimide ring opening (222-251 SCDKTHTCPPCPAPELLGGPSVFLFPPKPK). In addition, higher amounts of deamidation on the light chain (+6%), isoAsp (D283 on the heavy chain, +17%) and pyroGlu (E1 on the heavy chain, +3%) were detected (Table 1).

SEC-nMS experiments—SEC-nMS was used first for the identification and quantification of degradation products. For forced degradation studies, SEC-nMS experiments are only performed on intact T-DXd, as information on thermally-generated HMWS and LMWS would be lost upon digestion. Interestingly, a slight shift in retention time is observed for the monomer (peak 2, 62%), which

might suggest that thermal stress induces a small conformational change of the ADC. The mass measured for the main monomeric species is strictly identical to the reference sample (156,339 ± 2 Da), with the same glycoforms profile. However, the presence of a minor form with two oxidations (156,376 ± 1 Da) is now detected along with the unmodified monomer (Table 2). More importantly, no signals corresponding to either unconjugated mAb or DAR <8 are observed, indicating that no deconjugation occurs upon forced degradation. Upon thermal stress, the amount of HMWS increases to 10%, and additional LMWS are detected on the right of the main peak (Fig. 3A). The hinge region is a known mAb degradation hotspot, and peak 3 (21%) corresponds to a series of Fc-Fab fragments comprising 6 drugs, with a continuum of cleavage sites in the upper hinge region D224/K/T/H/T/C229, as previously reported for another thermally-stressed IgG1-based ADC [54] (Table 2). The peak 4 (7%) contains dimeric and free light chain. By comparing T-DXd to its non-functionalized mAb trastuzumab in similar forced degradation conditions (thermal stress), we determined that T-DXd is more prone to degradation into LMWS than the naked mAb (~28% of LMWS compared to 5% for trastuzumab) and that T-DXd is more prone to aggregation (~5% HMWS) than trastuzumab (HMWS <1%). This result is in good agreement with several publications confirming that ADCs are more likely to generate degradation products than their parent non-functionalized mAb [54–56].

HICxSEC-nMS experiments—Significant retention time shifts in HIC chromatograms after thermal stress are used as indications to tackle drug deconjugation issues. Forced degradation of T-DXd does not impact the retention time at the intact level, and mass measurements are still in line with the mAb bearing 8 drugs (156,504 ± 13 Da), confirming that thermal stress does not induce drug deconjugation (Fig. 4A). However, the major chromatographic peak broadens (+0.7 min at FWHM), and the populations corresponding to the main monomer and H1 are partially overlapped, which suggest that multiple PTMs contribute to peak widening. For more in-depth investigation, we performed HIC-nMS at the middle-up level: forced degradation leads to an early retention shift for both the major Fc peak and the hydrophilic variant H1, without any mass modification (50,466 ± 2 Da for the main peak), which could correspond to an isoAsp and/or deamidation, as both PTMs can lower HIC retention times [41] (Fig. 4B). The main Fab peak is now eluted later (from ~46.0 to 47.4 min), but its mass remains strictly identical to the one measured for the non-stressed sample. As peptide mapping did not identify any isoAsp in the Fab region, and in light of SEC data, we hypothesize that the retention time delay might rather be explained by a conformational change occurring upon thermal stress, which could favor access to additional hydrophobic regions.

CEX-nMS experiments—As abovementioned, CEX-nMS experiments are expected to be more informative than HIC for the separation and identification of PTMs. At the intact level, the major peak broadens with a late shift in retention time (peak now centered on ~18.1 min, FWHM = 0.90 min, Fig. 5A). No mass shifts are observed compared to the non-stressed sample, which suggests that the amount of basic variants increases, and/or that a conformational rearrangement happens upon heat exposure, giving access to additional surface charges. The amount of oxidized species does not increase, in line with peptide mapping results. As intact-level CEX analyses of T-DXd are once again not highly conclusive, we moved to middle-level analysis. After IdeS digestion, only few peaks in the CEX chromatographic profile of T-DXd are impacted by high temperatures (Fig. 5B). Among PTMs that are commonly encountered and susceptible to increase upon thermal stress, isoAsp leads to late retention shift, while deamidation induces an early shift in retention time [41]. The Fc region exhibits two newly-generated acidic variants, corresponding to one (A1) and two deamidations (A2, one on each Fc/2) (Table 3B). Based on peptide mapping performed on the stressed sample, the deamidation site is localized at N328. Of note, additional early-eluting species (not shown on the chromatogram) corresponding to free and dimeric light chain were also observed after thermal stress, in agreement with fragments identified with SEC-nMS.

4. Conclusions

As exemplified by T-DXd, the characterization of biopharmaceuticals is challenging and multiple analytical strategies need to be combined to have a global view of the micro-heterogeneity of mAbs or ADCs. SEC, HIC, and CEX are orthogonal techniques that separate size, hydrophobic, and charge variants, respectively, from the major protein isoform. Advantages and limitations of those techniques are summarized in Table 4.

Among these chromatographic methods, SEC is the most straightforward to couple with nMS. By combining the fast-online desalting and separation capabilities of SEC with the high mass accuracy of nMS, unambiguous species identification and drug load quantification can be rapidly achieved without extensive sample preparation. SEC-nMS provides a direct snapshot of the heterogeneity/homogeneity of drug conjugation, which makes it particularly interesting to perform routine analyses on ADCs to quickly conclude on conjugation efficiency. For ADCs, performing SEC-nMS at the intact level is usually enough to provide accurate characterization of the main drug substance product along with its HMWS and LMWS (including for forced degradation studies), especially with the recent development of new bioinert SEC columns which afford better separation and subsequent quantification of all species [43]. Of course, middle-up level experiments can also be performed to better localize drug conjugation sites.

Table 3. CEX-nMS mass measurements of T-DXd at intact and middle-up levels.

(A) INTACT LEVEL				(B) MIDDLE-UP LEVEL			
Charge variant			Experimental mass (Da)	Charge variant			Experimental mass (Da)
M		G0F-N/G0F	156,137 ± 5 Da	**Fc**		G0F-N/G0F	50,261.2 ± 0.9 Da
		G0F/G0F	156,339 ± 1 Da			G0F/G0F	50,463.8 ± 0.2 Da
		G1F/G0F	156,499 ± 3 Da			G1F/G0F	50,625.0 ± 0.3 Da
		G1F/G1F	156,661 ± 2 Da			G1F/G1F	50,787.1 ± 0.1 Da
A1	1 oxidation	G0F/G0F	156,353 ± 1 Da	**A1**	1 deamidation		50,465.1 ± 0.6 Da
		G1F/G0F	156,515 ± 1 Da	**A2**	2 deamidations		50,466.3 ± 0.3 Da
		G1F/G1F	156,678 ± 4 Da	**B1**	1 isoAsp?		50,464.0 ± 0.3 Da
A2	2 oxidations	G0F/G0F	156,371 ± 1 Da	**B2**	1 oxidation	G0F/G0F	50,480.0 ± 0.5 Da
		G1F/G0F	156,536 ± 3 Da	**B3**	+K (C-term)		50,592.5 ± 0.7 Da
		G1F/G1F	156,697 ± 6 Da	**B4**	+2K (C-term)		50,720.7 ± 1.1 Da
B1	1 isoAsp?	G0F/G0F	156,339 ± 4 Da	**B5**	2 oxidations		50,496.2 ± 0.6 Da
		G1F/G0F	156,500 ± 7 Da	**Fab**		-	52,953.6 ± 0.2 Da
		G1F/G1F	156,660 ± 6 Da	**A'1**	1 oxidation		52,972.1 ± 0.7 Da
				A'2	2 deamidations		52,955.4 ± 0.2 Da
				B'1	1 pyroGlu		52,936.0 ± 0.4 Da

Additional species generated upon thermal stress are reported in orange. Acidic variants are indicated with the letter A and basic variants with the letter B. For Fc variants, only masses corresponding to the main glycoform (G0F/G0F) are indicated.

Table 4. Pros and cons of non-denaturing LCs coupled to nMS.

	Separation based on	Main type of information obtained	LC sensitivity	Ease of coupling to nMS	Advantages	Drawbacks
SEC	Hydrodynamic volume	Size variants avDAR DLD Amount of unconjugated mAb	–	++	Speed Improved desalting efficiency Low injected quantities Use of volatile aqueous buffers	Sample diluted Secondary interactions with stationary phase (electrostatic and hydrophobic)
HIC	Hydrophobicity	Hydrophobicity-related PTMs avDAR Cys-ADC characterization	+	–	Detection of hydrophobic species	High salt concentrations Salting out effect Separation of DAR species only efficient for ADCs bearing hydrophobic drugs
IEX	Net apparent charge	Charge-related PTMs	++	+	Highly selective May separate conformers if their solvent-accessible charges are different	mAbs/ADCs with high PIs eluted at high salt concentrations High-resolution MS recommended for higher confidence in PTM identification pH dependent: Minor changes to mobile phases impact the IEX profile Secondary interactions with stationary phase (electrostatic and hydrophobic)

We believe that SEC-nMS on intact mAb-based formats is mature enough to be implemented as first line analysis, providing more information (HMWS, LMWS, main product) than rpLC-MS within a single analysis in few minutes (from 5 to 15 min per sample on 3–15 cm SEC columns). New generation of benchtop ready-to-use LC-MS instrumentations allow automation of all steps of the analysis, from online sample desalting to nMS analysis, data treatment, and even reporting. SEC-nMS analysis requires few micrograms of sample to be injected (limit of detection of 0.1 μg, classical injected amounts ranging between 10–50 μg) [57].

CEX-nMS is a particularly powerful technique to tackle charge variants, which ideally complements size variants characterization obtained through SEC-nMS. Easy-to-use CEX-nMS methods have now been largely described [46]. It is possible to achieve a straightforward and fast analysis ($<$10 min with 5-cm CEX columns) for a large variety of mAb-based formats, with MS identification of even minor species. However, it should be noted that intact-level CEX-nMS experiments are generally not sufficient for the unambiguous determination of small PTMs ($\leq$1 Da, *e.g.*, deamidation and isoAsp), even with high-resolution Orbitrap detectors. Although middle-up level CEX-nMS gives stronger confidence in PTM identification, we still recommend here peptide mapping to be carried out in parallel for unambiguous PTM confirmation and subsequent amino acid localization [46].

Despite the success in SEC- and CEX-nMS couplings, the implementation of a HIC-nMS method remains highly challenging due to the high salt concentration in the mobile phase required for optimal chromatographic separation. As 2D LC setups are required to online-couple HIC to nMS without compromising chromatographic separation, the MS sampling is limited by the run time of the second dimension, thus hampering the differentiation of closely-eluted species separated in the first HIC dimension. Additionally, 2D LC workflows significantly dilute samples along the elution, which can result in low MS intensities that prevent the identification of variants. We thus believe this coupling still requires further method development.

In conclusion, our results clearly highlight the benefits of non-denaturing LC coupled to nMS (especially SEC and CEX) over more conventional rpLC-MS analysis in denaturing conditions for the characterization of Cys-linked ADCs, and more generally for mAb-based products. These methods allow the characterization of the ADC in terms of DLD, avDAR, and the amount of unconjugated mAb (SEC) while providing valuable information about the relative quantification of sequence variants that modify the surface charge (CEX) and/or the apparent hydrophobicity (HIC) of the mAb. Furthermore, aggregation or fragmentation tendencies of these proteins can be also inferred from the combination of SEC with nMS. In spite of the specific limitations associated to each individual technique, the study of T-DXd clearly illustrates the complementarity of these separation methods to provide a complete characterization of the heterogeneous structure of ADCs with high-throughput and avoiding introduction of artifactual modifications that can typically occur when mAb-derived proteins are subjected to enzymatic digestions.

Author Contributions

ED, OH-A and SC designed the research study. ED, SE and HD performed the experiments. ED and HD analyzed the data. AD, PC and XP provided samples. ED and SC wrote the manuscript. All authors contributed to editorial changes in the manuscript. All authors read and approved the final manuscript.

Ethics Approval and Consent to Participate

Not applicable.

Acknowledgment

Mass spectrometers were purchased through financial support of GIS IBiSA (Synapt G2 HDMS), Région Grand Est (Orbitrap Exactive Plus EMR), and ProFI (maXis II and Orbitrap Q Exactive Plus). ED acknowledges the French Ministry for Education and Research for funding her PhD. PC, XP, and AD acknowledge the collaboration with Aerocom for this research project.

Funding

This study was supported by the CNRS, the University of Strasbourg, the Agence Nationale de la Recherche, and the French Proteomic Infrastructure (ProFI; ANR-10-INBS-08-03), the Interdisciplinary Thematic Institute IMS (Institut du Médicament Strasbourg), as part of the ITI 2021-2028 supported by IdEx Unistra (ANR-10-IDEX-0002), and by SFRI-STRAT'US project (ANR-20-SFRI-0012).

Conflict of Interest

The authors declare no conflict of interest.

Supplementary Material

Supplementary material associated with this article can be found, in the online version, at https://doi.org/10.31083/j.fbl2710290.

References

[1] Joubert N, Beck A, Dumontet C,Denevault-Sabourin C. Antibody–Drug Conjugates: The Last Decade. Pharmaceuticals. 2020; 13: 245.

[2] Dean AQ, Luo S, Twomey JD, Zhang B. Targeting cancer with antibody-drug conjugates: Promises and challenges. mAbs. 2021; 13: 1951427.

[3] Kaplon H, Chenoweth A, Crescioli S, Reichert JM. Antibodies to watch in 2022. mAbs. 2022; 14: 2014296.

[4] Agarwal P, Bertozzi CR. Site-Specific Antibody–Drug Conjugates: the Nexus of Bioorthogonal Chemistry, Protein Engineer-

ing, and Drug Development. Bioconjugate Chemistry. 2015; 26: 176–192.
[5] Vankemmelbeke M, Durrant L. Third-generation antibody drug conjugates for cancer therapy – a balancing act. Therapeutic Delivery. 2016; 7: 141–144.
[6] Beck A, Goetsch L, Dumontet C, Corvaïa N. Strategies and challenges for the next generation of antibody–drug conjugates. Nature Reviews Drug Discovery. 2017; 16: 315–337.
[7] Lyon RP, Bovee TD, Doronina SO, Burke PJ, Hunter JH, Neff-LaFord HD, *et al*. Reducing hydrophobicity of homogeneous antibody-drug conjugates improves pharmacokinetics and therapeutic index. Nature Biotechnology. 2015; 33: 733–735.
[8] Donaghy H. Effects of antibody, drug and linker on the preclinical and clinical toxicities of antibody-drug conjugates. mAbs. 2016; 8: 659–671.
[9] van Berkel SS, van Delft FL. Enzymatic strategies for (near) clinical development of antibody-drug conjugates. Drug Discovery Today: Technologies. 2018; 30: 3–10.
[10] Matsuda Y, Mendelsohn BA. An overview of process development for antibody-drug conjugates produced by chemical conjugation technology. Expert Opinion on Biological Therapy. 2020; 21: 963–975.
[11] Walsh SJ, Bargh JD, Dannheim FM, Hanby AR, Seki H, Counsell AJ, *et al*. Site-selective modification strategies in antibody–drug conjugates. Chemical Society Reviews. 2021; 50: 1305–1353.
[12] Fu Z, Li S, Han S, Shi C, Zhang Y. Antibody drug conjugate: the "biological missile" for targeted cancer therapy. Signal Transduction and Targeted Therapy. 2022; 7: 93.
[13] Nakada T, Masuda T, Naito H, Yoshida M, Ashida S, Morita K, *et al*. Novel antibody drug conjugates containing exatecan derivative-based cytotoxic payloads. Bioorganic and Medicinal Chemistry Letters. 2016; 26: 1542–1545.
[14] Ogitani Y, Aida T, Hagihara K, Yamaguchi J, Ishii C, Harada N, *et al*. DS-8201a, a Novel HER2-Targeting ADC with a Novel DNA Topoisomerase i Inhibitor, Demonstrates a Promising Antitumor Efficacy with Differentiation from T-DM1. Clinical Cancer Research. 2016; 22: 5097–5108.
[15] Cortés J, Kim S, Chung W, Im S, Park YH, Hegg R, *et al*. Trastuzumab Deruxtecan versus Trastuzumab Emtansine for Breast Cancer. New England Journal of Medicine. 2022; 386: 1143–1154.
[16] Lewis Phillips GD, Li G, Dugger DL, Crocker LM, Parsons KL, Mai E, *et al*. Targeting HER2-Positive Breast Cancer with Trastuzumab-DM1, an Antibody–Cytotoxic Drug Conjugate. Cancer Research. 2008; 68: 9280–9290.
[17] Rathore D, Faustino A, Schiel J, Pang E, Boyne M, Rogstad S. The role of mass spectrometry in the characterization of biologic protein products. Expert Review of Proteomics. 2018; 15: 431–449.
[18] Kaur H, Beckman J, Zhang Y, Li ZJ, Szigeti M, Guttman A. Capillary electrophoresis and the biopharmaceutical industry: Therapeutic protein analysis and characterization. TrAC Trends in Analytical Chemistry. 2021; 144: 116407.
[19] Füssl F, Strasser L, Carillo S, Bones J. Native LC–MS for capturing quality attributes of biopharmaceuticals on the intact protein level. Current Opinion in Biotechnology. 2021; 71: 32–40.
[20] Neupane R, Bergquist J. Analytical techniques for the characterization of Antibody Drug Conjugates: Challenges and prospects. European Journal of Mass Spectrometry. 2017; 23: 417–426.
[21] Hengel SM, Sanderson R, Valliere-Douglass J, Nicholas N, Leiske C,Alley SC. Measurement of in Vivo Drug Load Distribution of Cysteine-Linked Antibody–Drug Conjugates Using Microscale Liquid Chromatography Mass Spectrometry. Analytical Chemistry. 2014; 86: 3420–3425.
[22] Ehkirch A, Hernandez-Alba O, Colas O, Beck A, Guillarme D, Cianférani S. Hyphenation of size exclusion chromatography to native ion mobility mass spectrometry for the analytical characterization of therapeutic antibodies and related products. Journal of Chromatography. B, Analytical Technologies in the Biomedical and Life Sciences. 2018; 1086: 176–183.
[23] Friese OV, Smith JN, Brown PW, Rouse JC. Practical approaches for overcoming challenges in heightened characterization of antibody-drug conjugates with new methodologies and ultrahigh-resolution mass spectrometry. mAbs. 2018; 10: 335–345.
[24] Jones J, Pack L, Hunter JH, Valliere-Douglass JF. Native size-exclusion chromatography-mass spectrometry: suitability for antibody–drug conjugate drug-to-antibody ratio quantitation across a range of chemotypes and drug-loading levels. mAbs. 2019; 12: 1682895.
[25] Chen B, Lin Z, Alpert AJ, Fu C, Zhang Q, Pritts WA, *et al*. Online Hydrophobic Interaction Chromatography–Mass Spectrometry for the Analysis of Intact Monoclonal Antibodies. Analytical Chemistry. 2018; 90: 7135–7138.
[26] Wei B, Han G, Tang J, Sandoval W, Zhang YT. Native Hydrophobic Interaction Chromatography Hyphenated to Mass Spectrometry for Characterization of Monoclonal Antibody Minor Variants. Analytical Chemistry. 2019; 91: 15360–15364.
[27] Yan Y, Xing T, Wang S, Daly TJ, Li N. Online coupling of analytical hydrophobic interaction chromatography with native mass spectrometry for the characterization of monoclonal antibodies and related products. Journal of Pharmaceutical and Biomedical Analysis. 2020; 186: 113313.
[28] Ehkirch A, D'Atri V, Rouviere F, Hernandez-Alba O, Goyon A, Colas O, *et al*. An Online Four-Dimensional HIC×SEC-IM×MS Methodology for Proof-of-Concept Characterization of Antibody Drug Conjugates. Analytical Chemistry. 2018; 90: 1578–1586.
[29] Zhang Z, Zhou S, Han L, Zhang Q, Pritts WA. Impact of linker-drug on ion exchange chromatography separation of antibody-drug conjugates. mAbs. 2019; 11: 1113–1121.
[30] Matsuda Y, Kliman M, Mendelsohn BA. Application of Native Ion Exchange Mass Spectrometry to Intact and Subunit Analysis of Site-Specific Antibody–Drug Conjugates Produced by AJICAP first Generation Technology. Journal of the American Society for Mass Spectrometry. 2020; 31: 1706–1712.
[31] Marcoux J, Champion T, Colas O, Wagner-Rousset E, Corvaïa N, Van Dorsselaer A, *et al*. Native mass spectrometry and ion mobility characterization of trastuzumab emtansine, a lysine-linked antibody drug conjugate. Protein Science. 2015; 24: 1210–1223.
[32] Debaene F, Bœuf A, Wagner-Rousset E, Colas O, Ayoub D, Corvaïa N, *et al*. Innovative Native MS Methodologies for Antibody Drug Conjugate Characterization: High Resolution Native MS and IM-MS for Average DAR and DAR Distribution Assessment. Analytical Chemistry. 2014; 86: 10674–10683.
[33] Chevreux G, Tilly N, Bihoreau N. Fast analysis of recombinant monoclonal antibodies using IdeS proteolytic digestion and electrospray mass spectrometry. Analytical Biochemistry. 2011; 415: 212–214.
[34] Sjögren J, Olsson F, Beck A. Rapid and improved characterization of therapeutic antibodies and antibody related products using IdeS digestion and subunit analysis. The Analyst. 2016; 141: 3114–3125.
[35] Faid V, Leblanc Y, Bihoreau N, Chevreux G. Middle-up analysis of monoclonal antibodies after combined IgdE and IdeS hinge proteolysis: Investigation of free sulfhydryls. Journal of Pharmaceutical and Biomedical Analysis. 2018; 149: 541–546.
[36] Khalili H. Using different proteolytic enzymes to digest antibody and its impact on stability of antibody mimetics. Journal of Immunological Methods. 2021; 489: 112933.

[37] Beck A, Diemer H, Ayoub D, Debaene F, Wagner-Rousset E, Carapito C, *et al*. Analytical characterization of biosimilar antibodies and Fc-fusion proteins. TrAC Trends in Analytical Chemistry. 2013; 48: 81–95.
[38] Spanov B, Olaleye O, Lingg N, Bentlage AEH, Govorukhina N, Hermans J, *et al*. Change of charge variant composition of trastuzumab upon stressing at physiological conditions. Journal of Chromatography A. 2021; 1655: 462506.
[39] Harris RJ, Kabakoff B, Macchi FD, Shen FJ, Kwong M, Andya JD, *et al*. Identification of multiple sources of charge heterogeneity in a recombinant antibody. Journal of Chromatography B: Biomedical Sciences and Applications. 2001; 752: 233–245.
[40] Zheng K, Chen Y, Wang J, Zheng L, Hutchinson M, Persson J, *et al*. Characterization of Ring-Opening Reaction of Succinimide Linkers in ADCs. Journal of Pharmaceutical Sciences. 2019; 108: 133–141.
[41] Xu Y, Wang D, Mason B, Rossomando T, Li N, Liu D, *et al*. Structure, heterogeneity and developability assessment of therapeutic antibodies. mAbs. 2018; 11: 239–264.
[42] Haberger M, Leiss M, Heidenreich A, Pester O, Hafenmair G, Hook M, *et al*. Rapid characterization of biotherapeutic proteins by size-exclusion chromatography coupled to native mass spectrometry. mAbs. 2015; 8: 331–339.
[43] Murisier A, Andrie M, Fekete S, Lauber M, D'Atri V, Iwan K, *et al*. Direct coupling of size exclusion chromatography and mass spectrometry for the characterization of complex monoclonal antibody products. Journal of Separation Science. 2022; 45: 1997–2007.
[44] Jefferis R. Posttranslational Modifications and the Immunogenicity of Biotherapeutics. Journal of Immunology Research. 2016; 2016: 1–15.
[45] Bailey AO, Han G, Phung W, Gazis P, Sutton J, Josephs JL, *et al*. Charge variant native mass spectrometry benefits mass precision and dynamic range of monoclonal antibody intact mass analysis. mAbs. 2018; 10: 1214–1225.
[46] Murisier A, Duivelshof BL, Fekete S, Bourquin J, Schmudlach A, Lauber MA, *et al*. Towards a simple on-line coupling of ion exchange chromatography and native mass spectrometry for the detailed characterization of monoclonal antibodies. Journal of Chromatography A. 2021; 1655: 462499.
[47] Morty RE, Diepold K, Bomans K, Wiedmann M, Zimmermann B, Petzold A, *et al*. Simultaneous Assessment of Asp Isomerization and Asn Deamidation in Recombinant Antibodies by LC-MS following Incubation at Elevated Temperatures. PLoS ONE. 2012; 7: e30295.
[48] Dada OO, Jaya N, Valliere-Douglass J, Salas-Solano O. Characterization of acidic and basic variants of IgG1 therapeutic monoclonal antibodies based on non-denaturing IEF fractionation. Electrophoresis. 2015; 36: 2695–2702.
[49] Yan Y, Liu AP, Wang S, Daly TJ, Li N. Ultrasensitive Characterization of Charge Heterogeneity of Therapeutic Monoclonal Antibodies Using Strong Cation Exchange Chromatography Coupled to Native Mass Spectrometry. Analytical Chemistry. 2018; 90: 13013–13020.
[50] Leblanc Y, Ramon C, Bihoreau N, Chevreux G. Charge variants characterization of a monoclonal antibody by ion exchange chromatography coupled on-line to native mass spectrometry: Case study after a long-term storage at +5 °C. Journal of Chromatography B. 2017; 1048: 130–139.
[51] Wagner-Rousset E, Fekete S, Morel-Chevillet L, Colas O, Corvaïa N, Cianférani S, *et al*. Development of a fast workflow to screen the charge variants of therapeutic antibodies. Journal of Chromatography A. 2017; 1498: 147–154.
[52] Fekete S, Beck A, Veuthey J, Guillarme D. Ion-exchange chromatography for the characterization of biopharmaceuticals. Journal of Pharmaceutical and Biomedical Analysis. 2015; 113: 43–55.
[53] Nowak C, Cheung JK, Dellatore SM, Katiyar A, Bhat R, Sun J, *et al*. Forced degradation of recombinant monoclonal antibodies: A practical guide. MAbs. 2017; 9: 1217–1230.
[54] Deslignière E, Ehkirch A, Duivelshof BL, Toftevall H, Sjögren J, Guillarme D, *et al*. State-of-the-Art Native Mass Spectrometry and Ion Mobility Methods to Monitor Homogeneous Site-Specific Antibody-Drug Conjugates Synthesis. Pharmaceuticals. 2021; 14: 498.
[55] Wakankar AA, Feeney MB, Rivera J, Chen Y, Kim M, Sharma VK, *et al*. Physicochemical Stability of the Antibody−Drug Conjugate Trastuzumab-DM1: Changes due to Modification and Conjugation Processes. Bioconjugate Chemistry. 2010; 21: 1588–1595.
[56] Mohamed HE, Mohamed AA, Al-Ghobashy MA, Fathalla FA, Abbas SS. Stability assessment of antibody-drug conjugate Trastuzumab emtansine in comparison to parent monoclonal antibody using orthogonal testing protocol. Journal of Pharmaceutical and Biomedical Analysis. 2018; 150: 268–277.
[57] VanAernum ZL, Busch F, Jones BJ, Jia M, Chen Z, Boyken SE, *et al*. Rapid online buffer exchange for screening of proteins, protein complexes and cell lysates by native mass spectrometry. Nature Protocols. 2020; 15: 1132–1157.